SLAC-PUB-80
March 1965

# BEAM DYNAMICS PROBLEMS IN A HIGH-ENERGY ELECTRON LINAC*

G. A. Loew and R. H. Helm
Stanford Linear Accelerator Center
Stanford University, Stanford, California

## Introduction

In Stage I, with 240 klystrons and 960 accelerator sections, the Stanford Linear Accelerator is expected to produce an electron beam with the basic specifications outlined in Table I. The purpose of this paper is to review the characteristics of the beam as it travels along the two-mile length from the injector to the beam switchyard leading to the various end stations. The injector and the switchyard, however, are the subjects of separate papers[1,2]. The overall two-mile course of the beam is illustrated in Fig. 1 which emphasizes the various systems involved in beam guidance and diagnostics. It also shows the location of a positron source and future additional injectors.

The paper will begin with a discussion of the beam dynamics for an ideal accelerator. It will then describe the longitudinal and transverse properties of the beam in a real machine and examine the effects and cures of various types of imperfections. This discussion will be followed by a description of the diagnostic equipment needed to measure the characteristics of the beam and to determine the proper corrective actions. Finally, there will be a discussion of operational procedures to set up simultaneous beams of different energies and currents.

## Beam Dynamics of an Ideal Accelerator

We shall assume from the outset that the electrons from the injector are already fairly relativistic – e.g., $\gamma > 20$ – and that the longitudinal and transverse phase spaces are small.

The electromagnetic field in a disk-loaded waveguide is of the circularly symmetric TM type, for which by definition $B_z = B_r = E_\varphi = 0$. The remaining components are given, to first order in the transverse coordinates, by

$$E_z = E(z,t) + \ldots,\quad E_r = -\frac{r}{2}\frac{\partial E}{\partial z} + \ldots,\quad B_\varphi = \frac{r}{2}\frac{1}{c}\frac{\partial E}{\partial t} + \ldots$$

where $E(z,t) = E_z(0,0,z,t)$ is the accelerating field along the axis. If we calculate the Lorentz force of this field, the equations of motion of an electron to first order in the transverse coordinates are

$$\frac{d\gamma}{dz} = E(z,t) \tag{1}$$

$$c\frac{dt}{dz} = \frac{1}{\beta} = \frac{\gamma}{\sqrt{\gamma^2 - 1}} \tag{2}$$

$$\frac{d}{dz}\left(\beta\gamma\frac{d\vec{x}_\perp}{dz}\right) = -\frac{\vec{x}_\perp}{2}\left(\frac{1}{\beta}\frac{\partial E}{\partial z} + \frac{1}{c}\frac{\partial E}{\partial t}\right) \tag{3}$$

where $\vec{x}_\perp = (x,y)$. For convenience, fields have been expressed in units of $mc^2/e/cm = 0.511$ MV/cm.

Equation (2) shows the effect of relativity in freezing the velocity at $\beta \approx 1$ as energy becomes large; thus the transit time is $ct \approx ct_o + z/\beta$, and is nearly independent of energy. If now the field is a pure traveling wave, e.g., $E(z,t) = E(z - \beta_p ct)$ where $\beta_p$ is the phase velocity, Eq. (1) becomes

TABLE I

SLAC BEAM SPECIFICATIONS FOR STAGE I

| | |
|---|---|
| Maximum energy V | ≈ 20 GeV |
| Relative energy spectrum width $\frac{\Delta V}{V}$ at half of maximum current | 1% |
| Typical peak current $i_{pk}$ | ≈ 50 mA |
| Typical average current $i_{av}$ | ≈ 30 μA or $2 \times 10^{14}$ electrons/sec |
| Current pulse length | Adjustable within 0.020 and 2.1 μsec |
| Repetition rate | 1, 60, 120, 180, 240, 300 and 360 pps |
| Peak current for very short pulses $i_{pk}$ | ≈ 1 amp |
| Maximum bunch length | 5° |
| Beam radius, r, from injector | 0.5 cm |
| Minimum radial accelerator aperture | |
| Disk iris | 0.955 cm |
| Beam scraper | 0.855 cm |
| Radial phase space $(r \times p_r)$ from injector | $9 \times 10^{-3}$ mc-cm |
| Maximum allowable radial phase space $(r \times p_r)$ into beam switchyard | 2 mc-cm (at 20 GeV) or $0.5 \times 10^{-4}$ radian - cm |
| Maximum number of interlaced beams of different energies | 3 |

*Work supported by U. S. Atomic Energy Commission

(Submitted to IEEE Particle Accelerator Conference, Washington, D.C., March 10-12, 1965)

$$\frac{d\gamma}{dz} = E\left((1 - \beta_p/\beta)z - \beta_p c t_o\right)$$

so that the rate of energy gain is constant if we make the wave synchronous with the electron ($\beta_p = \beta \approx 1$). For a harmonic synchronous wave we obtain

$$\gamma = \gamma_o + z\, E_o \cos\theta$$

where $\theta$ is a constant phase angle between the electron and the wave crest.

If we evaluate the transverse Eq. (3) in the case of a pure traveling wave, we find

$$\frac{d}{dz}\left(\beta\gamma \frac{d\vec{x}_\perp}{dz}\right) = -\frac{\vec{x}_\perp}{2}\,\frac{1 - \beta\beta_p}{\beta}\,\frac{\partial E}{\partial z}$$

For the nonrelativistic case ($\beta < 1$), the force term is the well known phase-dependent radial force. Thus, an electron leading the accelerating crest of the wave is in a region of negative $\partial E/\partial z$ so that the force is positive and consequently defocusing; similarly, the region behind the crest is focusing. However, if the wave is synchronous with the electron, $1 - \beta\beta_p = 1 - \beta^2 = \gamma^{-2}$, so that the force soon becomes negligible as $\gamma$ becomes large.

To show the effect of deviations from a pure synchronous traveling wave, we may transform the derivative operators in Eq. (3) to obtain

$$\frac{d}{dz}\left(\beta\gamma \frac{d\vec{x}_\perp}{dz}\right) = -\frac{\vec{x}_\perp}{2}\left(\frac{1}{\beta\gamma^2}\frac{\partial E}{\partial z} + \beta\frac{dE}{dz}\right) \qquad (4)$$

The first term on the right of this equation becomes negligible at high energy because of the $\gamma^{-2}$ dependence. The second term, which contains a total derivative of E, tends to average to zero and in fact vanishes identically for a synchronous traveling wave. Thus the transverse equation becomes

$$\frac{d}{dz}\left(\gamma \frac{d\vec{x}_\perp}{dz}\right) \approx 0$$

which implies constant transverse momentum and logarithmically increasing radial size:

$$\vec{p}_\perp = \gamma \frac{d\vec{x}_\perp}{dz} = \vec{p}_{\perp o} = \text{constant}$$

$$\vec{x}_\perp = \vec{x}_{\perp o} + \frac{\vec{p}_{\perp o}}{E}\log\frac{\gamma}{\gamma_o}$$

where constant acceleration has been assumed.

From these idealized results which are valid for a single relativistic electron whose radial displacement and momentum are small, we see that the beam dynamics are quite straightforward. In practice, however, a long linear accelerator suffers from a number of imperfections. We shall now discuss the longitudinal and transverse effects of these imperfections and point out some specific remedies which will be used.

## Longitudinal Effects of Imperfections and Proposed Remedies

### Imperfect Bunching

Because of space charge and the limitations of the injector bunching system,[1] the angular phase spread $\alpha$ of the bunches in the accelerator remains finite. For simplicity, we shall assume that all electrons are contained within $\alpha$ and that their distribution is uniform. By inspection of Figs. 2a, it can be seen that this angular phase spread results in both an energy decrease and a finite spectrum width. This effect exists whether one considers an accelerator with a single section contributing an energy $V_n \cos\theta_n$ or the sum of N sections giving a total energy

$$V_N = \sum_0^N V_n \cos\theta_n .$$

This total energy can be understood as the projection of the vectorial sum $V_T$ on the axis represented by the injector phase. Hence $V_N = V_T \cos\theta$. The angle $\theta_n$ is the phase angle of the central electron in a bunch with respect to the wave crest. This angle is constant only in the case of perfect synchronism and no beam loading. Otherwise, it is an average, integrated over the length of a section. From Figs. 2b and 2c, it is seen that the resultant angle $\theta$ can be made equal to zero by causing the vector $V_T$ to be collinear with the injector phase. The result can be obtained by adjusting the phase of the injector, the phase of a Sector (32 10-foot accelerator sections), or the phase of a few individual klystrons. The eight klystrons of Sector 27 on the accelerator are being reserved for this purpose to obtain individual phase closure for multiple beams.

At the cost of some fractional loss of energy, it is always possible to achieve phase closure, i.e., to make $\theta \equiv 0$. However, for a given angle $\alpha$, the narrowest obtainable spectrum is limited by the value $\alpha^2/8$. If $\alpha = 1/10$ radian,

$$\left(\frac{\Delta V}{V}\right)_{opt} \approx 0.0012.$$

Under these conditions, the finite bunch size is obviously not the limiting factor to the specifications of Table I.

### Beam Loading

The effect contributing most to spectrum broadening is transient beam loading. The energy gain $V_n$ in a constant-gradient accelerator section of length $\ell$, input power $P_n$, shunt impedance per unit length $r$ and attenuation parameter $\tau$ is[3]

$$V_n = (1 - e^{-2\tau})^{\frac{1}{2}}\,(P_n \ell r)^{\frac{1}{2}} \cos\theta_{o,n} - \frac{ir\ell}{2}\left(1 - \frac{2\tau e^{-2\tau}}{1 - e^{-2\tau}}\right)$$

where $i$ is the peak beam current and $\theta_{o,n}$ is the phase angle of the electron with respect to the wave crest at the input. As discussed above, $\theta_n$ remains equal to $\theta_{o,n}$ in a given section if beam loading is negligible, or $\theta_n = \theta_{o,n} \equiv 0$ and if the phase velocity of the wave $v_p$ is equal to c. Otherwise, slippage occurs. The above formula holds only for perfect synchronism. If electron injection into a section starts after one filling time ($t_f = 2Q\tau/\omega = 0.83$ μsec for SLAC parameters), the electrons injected during the next interval $t_f$ will vary in energy by a maximum amount

$$\frac{ir\ell}{2}\left(1 - \frac{2\tau e^{-2\tau}}{1-e^{-2\tau}}\right)$$

All electrons injected after $t = 2t_f$ will be steady-state electrons having constant energy. For an rf pulse length of 2.5 μsec and an injector pulse length of 1.7 μsec, these constant energy electrons will only be contributed for $2.5 - 2(0.83) \approx 0.8$ μsec or roughly one-half of the injection pulse length. Assuming $P_n = 5$ MW, $i = 50$ mA and $\theta_{o,n} = 0$, the percentage decrease in energy between the first electron and those at steady state is 8%. Roughly, 40 to 50% of the electrons are outside the design spectrum width of 1%.

Several methods have been suggested[4] to reduce the effect of transient beam loading. The simplest to apply on a multi-klystron machine is to use a slightly longer injector pulse (2.1 μsec) and to "stagger-trigger" successive sectors of the accelerator in order to delay their rf turn-on time. Physically, this means that early electrons which normally would have excess energies of the order of 8% will pass through sections before these have been entirely filled with energy. With 30 sectors available, a fairly flexible "triggering program" can be developed with delays ranging, for example, from 0 to 0.9 $t_f$. A computer calculation has shown that by applying this staggered delay to approximately one-third of the sectors, it is possible to reduce the above spectrum width to less than 1%. Staggered triggering will also be useful in reducing the spectrum broadening caused by the effects mentioned below.

## Amplitude and Phase Modulation

There are three ways in which amplitude and phase modulation can contribute to a lowering of the maximum obtainable energy and to a broadening of the energy spectrum. The first arises simply from the fact that the output power of a klystron varies in amplitude and phase during a pulse and from pulse to pulse, predominantly because of the voltage instabilities of the high power modulators. Measurements on klystrons presently operating on the first two sectors of the accelerator show short-term voltage stabilities of approximately 0.1% and phase variations of no more than $1^\circ$ in the middle of the operating voltage range. The average phase ripple within a pulse is of the order of $\pm 2.5^\circ$ (see Figs. 3a and 3b). However, this ripple is not coherent from klystron to klystron and the resulting spectrum broadening is negligible. The second effect arises because the filter characteristics of the accelerator distort even a perfectly rectangular rf envelope input and cause it to develop amplitude and phase oscillations as it travels along each 10-foot accelerator section. This effect, first pointed out and studied theoretically by J. E. Leiss,[5] has been investigated experimentally[3] at SLAC. The third effect which further complicates the problem is that a perfectly rectangular modulator pulse in fact causes the klystron output to contain frequency modulation in the rise and fall time. Figures 3c and 3d show the resulting rf pulse and phase modulation at the output of the corresponding accelerator section. Since this effect is coherent from section to section, the best remedy to reduce spectrum broadening is to use "stagger-triggering" from sector to sector as described previously. As a result, an electron will see a "valley" in one sector and a "peak" in another and the total energy ripple will be smoothed out. Another method which experimentally has proved to reduce amplitude ripple by about 50% is to let the rf turn-on be governed by a low power p-i-n diode modulator upstream of the klystron rather than by the klystron itself. This result can be explained by the relatively low FM content of the diode pulse.

## Transverse Effects of Imperfections, and Proposed Remedies

### Transport System

Among the effects which influence the transverse quality of the beam, some, such as space charge, gas scattering and radial rf field forces are quite small; others, such as stray magnetic fields, misalignments, asymmetry in the rf couplers, and perhaps the beam breakup phenomenon are potentially serious. In order to contain the initial phase space of the beam and to help compensate for the various transverse effects, a focusing system is being provided. The main focusing system consists of 30 quadrupole triplets, one at the end of each sector (333-1/3 feet). The specifications of the triplets are summarized in Table II. In addition to the standard triplets, a number of special short triplets, consisting of the same quadrupoles closely spaced, are used. One short triplet is placed approximately 40 feet after the injector for the purpose of transporting the low energy beam, with relatively large divergence, through the remainder of Sector 1. Thirteen more of the short triplets follow the positron source station in Sector 11 at roughly exponentially increasing spacing, to match the large phase space of the positron beam into the sector-spaced standard triplets. Typical transport properties[6] of the system are listed in Table III.

The choice of triplets rather than doublets was based primarily on consideration of alignment tolerances.[7] The most critical triplet alignment is collinearity, or straightness of a line joining the magnetic centers of the three quadrupoles. For doublets the skewness, or angular aiming of the doublet axis relative to the beam axis, is most critical. It is felt that the internal alignment can be maintained by a suitably rigid and thermally stable support structure, but that it would be difficult to keep the structure aimed with the accuracy of about $10^{-5}$ radian required for doublets.

### Containment of Phase Space

The design specification for phase space emittance of the injector has been stated as $9 \times 10^{-3}$ mc-cm

expressed as the product of the semi-minor axes of an equivalent erect ellipse (see Fig. 4). Recent emittance measurements[1] on a test injector indicate that virtually all the beam is within this figure.

The limiting admittance of the accelerator occurs between the lens at the 40-foot point and the end of Sector 1, and is about 0.04 mc-cm (see Table III). This admittance is a factor of 4 larger than the injector emittance, and hence is sufficient to permit containment of the beam within about half the accelerator aperture.

TABLE II

TRIPLET SPECIFICATIONS

| | |
|---|---|
| Quadrupole effective lengths: | |
| Center quadrupole: | 8 inches |
| End quadrupoles: | 4 inches |
| Total effective lengths of triplets: | |
| Standard triplet: | 84.5 inches |
| Short triplet: | 26.0 inches |
| Quadrupole bore (diameter): | 1.200 inches |
| Maximum field at bore radius: | 1.5 kilogauss |
| Power dissipation at nominal field: | |
| 4-inch quadrupole: | 45 watts |
| 8-inch quadrupole: | 72 watts |
| Cooling: | Natural convection |

TABLE III

OPTICAL PROPERTIES OF FOCUSING SYSTEM

| | |
|---|---|
| Admittance at high energy and maximum quadrupole strength: | 0.6 mc-cm |
| Low energy cut-off at maximum quadrupole strength: | 2.1 GeV |
| Maximum admittance at 2 GeV (limited by sector-spacing of standard triplets): | 0.28 mc-cm |
| Low energy cut-off with admittance maximized at 2 GeV: | 1.4 GeV |
| Admittance, injector to 40-foot point: | $\approx$ 0.06 mc-cm |
| Admittance, 40-foot point to end of Sector 1: | $\approx$ 0.04 mc-cm |
| Admittance through Sector 2: | $\approx$ 0.14 mc-cm |
| Admittance of Positron Transport System: | $\approx$ 0.3 mc-cm |

Space Charge

The diverging effect of space charge, in the absence of positive ions, falls off as $\gamma^{-2}$ because of the cancellation of electric and magnetic forces, and consequently is negligible for a beam which has gotten through the injector and up to relativistic energies. Space charge neutralization by positive ions in the residual gas is estimated to be insignificant.

Gas Scattering

Residual gas in the accelerator can scatter the beam slightly.[8] At a pressure of $10^{-5}$ mm Hg, the entire length of the machine would contain about $10^{-7}$ radiation length of residual gas, which through multiple scattering would introduce transverse momenta on the order of $10^{-2}$ mc. Single nuclear Coulomb scattering events would scatter about 10% of the beam to transverse momenta greater than $10^{-2}$ mc. Thus these effects only increase the beam phase space by an amount comparable to the injector emittance.

Longitudinal Variations

Longitudinal variations in amplitude and phase of the accelerating wave have a transverse effect described by Eq. (4), which in the relativistic limit becomes[9]

$$\frac{d}{dz}\left(\gamma \frac{d\vec{x}_\perp}{dz}\right) = -\frac{\vec{x}_\perp}{2}\frac{dE}{dz} \qquad (5)$$

Fringing fields at the entrance and exit of accelerator sections may be thought of as delta-functions in $dE/dz$ and consequently are equivalent to thin lenses of focal length $f = \pm 2\gamma/E$ (diverging at exit; converging at entrance). For a "perfect" machine with no internal field variation, the exit fringe field thus would be equivalent to a diverging lens of focal length $|f| \approx 2L$ = twice the length of the machine, a quite negligible effect. A gap in the rf structure is equivalent to a very weak alternating-gradient doublet.

Periodic variations in the rf field may be treated by a smoothed-force approximation to Eq. (5),

$$\frac{d}{dz}\left(\gamma \frac{d\vec{x}_\perp}{dz}\right) = -\frac{\vec{x}_\perp}{4\gamma}\left(\overline{E^2} - \bar{E}^2\right) \qquad (6)$$

where the superior bar denotes an average over a period of the variation, along an electron trajectory. The combined effect of space-harmonics and periodic gaps is found to have a net focusing equivalent to a longitudinal magnetic field of about 80 gauss; the entire length of the machine would be equivalent to about 0.2 betatron wavelength and the admittance would be about 0.02 mc-cm.

Stray Magnetic Fields

Transverse magnetic fields along the accelerator can result from several causes: the earth's magnetic field, magnetized reinforcing steel in the concrete, structural steel and heavy equipment in the Klystron Gallery, power line fields and ground currents in the accelerator support girder. As an indication of the problem, a 2-GeV electron would be deflected 1 mm in 10,000 feet by an uncompensated field of $1.5 \times 10^{-5}$ gauss.

Magnetic compensation is effected by degaussing wires and magnetic shielding along the accelerator,[10] and by steering dipoles at the end of each sector. The design objective of the degaussing and shielding (see Fig. 5) is reduction of the stray fields to $< 10^{-4}$ gauss, averaged over a sector. The degaussing currents are independently adjustable at Sector intervals. The magnetic shield is important in reducing ac fields and longitudinal and temporal variations in the earth's field, and also relaxes the accuracy required for degaussing. The effective dc shielding factor is about 10, being limited by unavoidable gaps at waveguide and water connections.

The steering dipoles consist of Helmholtz-type coils rated at $\approx$ 2000 gauss-cm, equivalent to a 1.2 mc transverse momentum impulse. They provide a final correction for all magnetic and other uncompensated deflections. The steering dipoles are pulsable, but initially will be supplied only with direct current.

AC fields and ground currents have been minimized by careful balancing and grounding. Preliminary measurements show that stray fields from all causes are probably within tolerance.

Table IV lists some typical tolerances for magnetic effects[11] under two different quadrupole focusing settings: minimal, or just enough focusing to keep the beam within about 1 cm diameter, and moderate focusing corresponding to a low energy cutoff at about 1.4 GeV.

Quadrupole Misalignments

Figure 6 shows the components of triplet misalignment, and Table V lists approximate tolerances.[7] We should hasten to point out that the most critical misalignment, noncollinearity, is just equivalent to a net dipole field and hence can be cancelled by the steering dipoles. Thus the collinearity tolerance actually specifies the need for sufficient stability of the support system so that frequent steering adjustments will not be necessary. Parallel displacement of the entire triplet imparts a transverse impulse which is energy-dependent, and therefore cannot be completely compensated over the entire energy band (2 to 20 GeV) by a single steering adjustment. Corrections could be effected either by independent pulse-to-pulse steering (not contemplated) or by realignment of the triplet relative to the accelerator.

The triplets will be pre-aligned relative to their magnetic centers, on a rigid support structure (see Fig. 11). During this pre-alignment the mean triplet axis will be indexed relative to a laser-beam alignment target[12] in the support girder; also, exterior optical tooling target holders will be indexed to each quadrupole to permit later checking on the alignment within a triplet.

Accelerator Misalignments

The machine will be aligned initially to within 0.040 inch of a straight line. To accomplish this, the 10-foot accelerator sections are first prealigned on the 40-foot girder assemblies to a tolerance of 0.010 inch, using a system of optical tooling targets and telescopes; then after installation, the 40-foot assemblies will be aligned relative to the laser beam.[12] Thermal gradients in the housing can set up additional distortions between 40-foot support points, but these effects will be minimized if necessary, e.g., by use of insulation.

The main effect of the initial random misalignment of the accelerator subassemblies is simply a loss in effective aperture of perhaps 10% in radius. This effect is not serious for the electron beam, for which the radius can be kept within 0.5 cm by minimal focusing; for the positron beam the transmission, proportional to the fourth power of aperture, may be reduced appreciably. The misaligned accelerator sections also have a slight deflecting effect but this is estimated to be small.

Over a period of time, additional misalignments will build up, e.g., because of settlement and horizontal motions of the earth. DC steering through these misalignments will introduce dispersion between high and low energy beams. The triplet focusing could reduce this dispersion so that, for example, a first harmonic misalignment amplitude of several centimeters could be tolerated.

Coupler Asymmetry

The rf coupler is designed for mechanical simplicity and ruggedness without loss of useful length of accelerator (see Fig. 7a). However, it is inherently unsymmetric and tends to introduce an rf field asymmetry which can result in a transverse deflection. The dominant effect of the asymmetry is given by

$$\delta\vec{p}_\perp = \left(\frac{\lambda}{2\pi}\right)^2 \int \frac{1}{c}\frac{\partial}{\partial t}\vec{\nabla}_\perp E_z \, dz \qquad (7)$$

TABLE IV

TOLERANCES ON MAGNETIC EFFECTS*

| Perturbing Effect | Tolerances | |
|---|---|---|
| | Moderate Focusing | Minimal Focusing |
| Uniform transverse field on axis | $140 \times 10^{-5}$ gauss | $2.1 \times 10^{-5}$ gauss |
| Random sector-to-sector field variations on axis | $240 \times 10^{-5}$ gauss (r.m.s) | $8.5 \times 10^{-5}$ gauss (r.m.s) |
| Currents in 24-inch girder | | |
| dc | 4 amp | 0.06 amp |
| 60 cps** | 40 amp | 0.60 amp |

*The tolerances are set by allowing a maximum beam deflection of 1 mm.

**The shielding factor is ten times larger at 60 cps than dc because of skin effect in the copper accelerator pipe.

TABLE V

ALIGNMENT TOLERANCES* FOR SLAC TRIPLETS (see Fig.6)

| Type of Error | r.m.s Tolerance |
|---|---|
| Parallel displacement ($\epsilon$) | $7 \times 10^{-3}$ inch |
| Skewness, ($\epsilon'$) | |
| Entire triplet | $70 \times 10^{-3}$ inch |
| Each quadrupole | (large) |
| Non-collinearity, ($\epsilon''$) | $0.7 \times 10^{-3}$ inch |
| Z-rotation ($\psi$) | |
| Entire triplet | $> 1^{\circ}$ |
| Each quadrupole | $0.1^{\circ}$ |

*The tolerances are set by allowing a maximum beam deflection of 1 mm.

for a wave which is harmonic in time, where $\lambda$ is the free space wave length and the integral is over the coupler cavity along an electron trajectory.

Considering only the linear gradient, we obtain approximately

$$\delta p_x = \frac{E_o \lambda d}{4\pi a} \left\{ \frac{\Delta E}{E_o} \sin\theta + \Delta\varphi \cos\theta \right\} \qquad (8)$$

where d is the coupler length, a is the disk aperture radius, $E_o$ is the amplitude of $E_z$, $\theta$ is the phase angle of the electron relative to the crest, and $\Delta E$ and $\Delta\varphi$ are the total linear variations in the amplitude and phase angle, respectively, across the aperture diameter. Note that the amplitude asymmetry couples the phase spread of the electron bunch into a first-order spread in transverse momentum while the phase asymmetry produces an unidirectional deflection of the bunch (see also Fig. 7b). The tolerances are estimated to be on the order of $\Delta E/E_o < 0.1\%$ and $\Delta\varphi < 0.01^{\circ}$.

An attempt was made to develop a coupler which retained the desirable features of the present design – simplicity and minimum wasted length – but which would be free of the asymmetry effects. Figure 7c illustrates the approach used, namely, the offset aperture design. By this method, couplers with $\Delta E/E_o < 0.1\%$ were produced, but unfortunately a phase asymmetry of $\approx 1^{\circ}$ remained. Experiments aimed at reducing the phase asymmetry in this type of coupler have not been successful.

After consideration of numerous alternatives, the decision was made to alternate the orientation of the couplers. The scheme which has been adopted is the "baba – abab" configuration defined in Fig. 8a. A simple "ababab . . ." alternation is not used because it can lead to a cumulative offset of the beam, as may be seen by tracing the trajectory shown in Fig. 8b through the first "baba" grouping. This is a very small effect, equivalent to half the net transverse impulse from a single input-output coupler pair; however, deflections of several millimeters could have resulted under extreme conditions of negligible focusing and multiple beams of widely different energies. The beam offset and transverse momentum could be cancelled in any group of four accelerator sections by using a "baab" or "abba" configuration, but this happens to introduce an interference between input and output waveguide flanges which would have required shortening the accelerator sections.

The "baba – abab" configuration was adopted after a study of such factors as interferences of waveguide and water connections and impact in installation schedules. The cancellation of transverse deflection is not exact in this case but is approximate to the extent that each "baba" group is matched with an equally powered "abab" group.

## The Beam Break-Up Phenomenon

The discussion of beam dynamics in a linear electron accelerator would be incomplete without a few comments on the beam break-up phenomenon, even though it is not expected to occur for the combinations of currents and pulse lengths specified for this accelerator. Following a few years of investigations, it is now understood[13] that above a certain

current threshold, the current pulse breaks up as shown in Fig. 9a because the electron beam accelerated by the $TM_{01}$ mode sets up a transverse deflecting backward wave in the so-called $TM_{11}$-like mode as shown in Figs. 9b and 9c. Typically, various laboratories have reported that for a three-meter-long uniform S-Band structure, a beam of about 300 mA sets up a $TM_{11}$-like wave which in about 1 μsec breaks up the beam. At Stanford it has been found that the process can be triggered with a current of 70 mA by injecting about 800 watts of peak power at 4326 Mc/sec backwards into the output of a uniform accelerator section. The same result, however, could not be achieved at this power level with a SLAC constant-gradient section. Here the slow taper of the transverse cavity dimensions causes the $TM_{11}$-like dispersion diagrams to shift up in frequency as one moves in the downstream direction. As a result, the phase velocity changes for a given frequency (and vice-versa) and the beam-wave interaction becomes incoherent along the length of the structure. As a result beam break-up should not occur until one reaches higher currents. This was confirmed by experiments done at Hughes Aircraft.[14] These results, when normalized to SLAC parameters, would tend to indicate that it would take about 450 mA of peak current to break up the beam in about 2 μsec. Such currents and pulse length combinations are clearly in excess of the required SLAC specifications.

## BEAM GUIDANCE AND DIAGNOSTIC EQUIPMENT

The steering and focusing equipment described in the previous paragraph, and the beam guidance and diagnostic equipment discussed below, are installed in the last ten feet of each 333-foot sector. These ten-foot lengths, each supported by an independent girder, are called "drift sections." The guidance and diagnostic equipment comprises beam position and intensity monitors, profile monitors, and collimators called "beam scrapers." Figure 10 shows an overall layout of a complete drift section.

### Beam Position and Intensity Monitors

Figure 11 shows a top view of a cylindrically symmetric phase reference cavity ($TM_{010}$ mode), two rectangular position cavities rotated by 90° with respect to each other ($TM_{120}$ mode), and a current monitor consisting of a transformer whose primary is the beam and whose secondary is a ferrite toroid with 25 turns of wire feeding into a load. The operation of the system can be understood by referring to the electric field patterns shown at the top of the figure. When the bunched beam traverses the three resonant cavities, it excites in them rf signals at 2856 Mc/sec whose magnitudes and phases depend on the field intensity and sign at the location of the center of charge of the beam. Hence, in the $TM_{010}$ cavity, the power induced is essentially independent of position and the phase is constant and equal to that of the beam. For a given coupling parameter $\beta$, the output power is given by the expression

$$P_{out} = 2\left(\frac{R}{Q}\right) Q_L \frac{\beta}{1+\beta} M^2 I^2 \qquad (9)$$

where $\frac{R}{Q}$ depends on the geometry of the cavity, $Q_L$ is the loaded $Q$ of the cavity, $M$ is the transit time factor, and $I$ is the peak beam current. Typical cavity parameters are given in the figure ($\beta = 7$, $M^2 \approx 0.67$).

Similarly, for the $TM_{120}$ position cavities, the output power is given by

$$P_{out}\begin{bmatrix} x \\ y \end{bmatrix} = \frac{4}{\pi}\frac{b}{a}\frac{\lambda_o}{\lambda_g}\eta Q_L \frac{\beta}{1+\beta} M^2 I^2 \sin^2\frac{2\pi}{\lambda_g}\begin{bmatrix} x \\ y \end{bmatrix} \qquad (10)$$

where $\eta$ is the free space impedance, $b$ is the cavity height, $a$ is the width, $\lambda_g$ is the guide wavelength, and $x$ and $y$ are the respective beam coordinates. Typical cavity parameters are also shown in the figure ($\beta > 10$, $M^2 \approx 0.47$).

The $TM_{010}$ cavity is used for several functions. A fraction of its output power drives a linear thermionic diode whose output current is integrated and gives the value of the charge $Q$ per pulse. Another fraction of its output power is split into two parts each of which is fed into a phase bridge which compares its phase with that from one of the $TM_{120}$ cavities. As the beam passes through the center of these cavities, the induced signal goes through zero and changes phase by 180°. By using two linear thermionic detectors per phase bridge, it is possible to derive a signal proportional to Ix or Iy which after integration gives Qx or Qy. A normalizing circuit yields the positions x and y. For each drift section, these signals together with a signal proportional to log $Q$ are sent to the Central Control Console over a so-called "baseband" system, discussed in another paper. Similarly, the output current of the toroid circuit is integrated and sent to Central Control as $Q$ over an accurate (1%) FM system. All these signals are displayed on oscilloscopes and meters and used by the Central Control Beam Operator to make his steering adjustments.

### Profile Monitors

To supplement the intensity and position information, appropriate space is being reserved on each drift section (see Fig. 10) for a beam profile monitor. A variety of systems have been contemplated. At the present time, there are three insertable 0.030" thick quartz Cerenkov radiators installed at the beginning of the accelerator with their respective TV viewing systems. Another monitor is presently being designed[15] which consists of a small (1 $mm^3$) Beryllium scattering target which scans the beam cross section through a bellows. The profile is obtained by displaying on a scope the output from an ion chamber placed downstream of the radiator, as a function of the target position obtained from the scanning mechanism.

### Collimators

At the downstream end of each drift section, there will be a collimator also called "beam scraper." The I.D. of this one-foot long copper cylinder is 0.673 in., i.e.,.080 in or 2 mm less than the smallest diameter of the accelerator sections. The design purpose of this device is to "scrape off" those peripheral electrons which are improperly focused and thereby to protect the disk-loaded waveguide from radiation damage. The water cooling system for each scraper has been designed to dissipate up to 15 kW on a continuous basis or as much

as the total beam power for the duration of one pulse, until the machine protection system shuts off the beam.

## Special Equipment for the Positron Source

The positron source in Sector 11 is a complicated system which will not be described here. However, it is of interest to briefly mention some special equipment related to the positron beam dynamics. The 13 special triplets have already been mentioned above. In addition, there will be some special profile and current monitors, just upstream and downstream of the positron radiator. A special precaution has to be taken to preserve the usefulness of some of the standard diagnostic equipment: as the positrons and electrons are produced in pairs, a good fraction of the electrons will be captured and accelerated within $\lambda_o/2$ of the positron bunches. The effect of these electrons would be additive for all microwave detectors and subtractive for the toroid current monitors. Rather than building complicated equipment such as second harmonic cavities to correct the readings, it has been decided to install a half-meter long rf deflector structure downstream of the positron radiator. This structure[16] which propagates a "$TM_{11}$-like" mode at 2856 Mc/sec is designed to produce a transverse momentum of 0.5 MeV/c. Its effect added to that of a pulsed magnet producing equal transverse momentum is to deflect the electrons (or the positrons, if the deflector phase is shifted by 180° or the magnetic field is reversed) into the accelerator wall within 10 feet and leave the positrons undisturbed.

## Beam Analyzing Stations

In addition to the regular drift sections, two momentum spectrometers have been installed, one permanently at the 30-foot point in Sector 1 and one, temporarily, at the end of Sector 2. The first one is used to study the energy spectrum of the beam as it emerges from the injector and the first three accelerator sections which are individually powered by 24 MW klystrons klystrons. It has a 30° bending angle and a 32.9-inch bending radius. The second one is used to study overall performance of the beam obtained with Sectors 1 and 2. It is shown in Fig. 12 together with an incomplete drift section. It has a bending angle of 7.7° and a bending radius of 126.9 inches. It is with this spectrometer that recent measurements of a 1.32 GeV, 1.5% spectrum beam have been obtained.

## Conclusions and Operational Procedures

Early operational results with Sectors 1 and 2 of the two-mile accelerator are proving to be quite encouraging. The various beam dynamics effects discussed in this report appear to be controllable even though a temporary and incomplete injector is being used. The overall beam transport, guidance and phasing systems seem to be working correctly. However, one of the more challenging specifications, namely, the capability of multiple beams on an interlaced pulse-to-pulse basis, will not be tested until completion of the machine. While final operational plans are not yet firm, it is assumed that when two or three simultaneous beams of different energies and currents are to be used, a number of parameters will be pre-established by the beam operator before any beam is actually turned on. These will include the number of klystrons to be assigned to each beam, the respective programs for "stagger-triggering," the degaussing currents (to be derived from a magnetic measurements survey). Most of the quadrupoles may at first be left off. Then, an attempt will be made to transmit the lowest energy beam from the injector to the Beam Switchyard with the aid of the steering dipoles and the position and current monitors. At this point, the entire machine may be phased sector by sector, with the help of an automatic phasing system which has been developed. If possible, the other beams will then be turned on and a compromise adjustment of the steering currents will have to be achieved to transmit all beams at the same time. Finally, to improve overall transmission, all quadrupoles may be turned on in a systematic way with the help of the profile monitors. If multiple beams cannot be transmitted, new adjustments may have to be made, including realignment of the machine. Finally, it may become necessary to equip at least a few of the dipoles with pulsed power supplies.

## Acknowledgments

The authors are indebted to the staff of the Accelerator Physics Department at SLAC for furnishing many of the experimental results used in this report.

## List of References

1. R. Miller, R. Koontz and D. Tsang, "The SLAC Injector," Paper H-8 of IEEE Particle Accelerator Conference, Washington, D.C., March 10-12, 1965.

2. R.E. Taylor, "Transport Systems for High Intensity Beams," Paper I-1 of IEEE Particle Accelerator Conference, Washington D.C., March 10-12, 1965.

3. A.L. Eldredge, G.A. Loew and R.B. Neal, "Design and Fabrication of the Accelerating Structure for the Stanford Two-Mile Accelerator," SLAC Report No. 7, Stanford Linear Accelerator Center, Stanford University, Stanford, California (1962).

4. K.L. Brown, et al., "Linear Electron Accelerator Progress at Stanford University," Proc. 1961 International Conference on High-Energy Accelerator, Brookhaven National Laboratory.

5. J.E. Leiss, National Bureau of Standards, Washington, D.C. (private communication).

6. R.H. Helm, "Optical Properties of Quadrupole Multiplets for Sector Focusing in the Two-Mile Accelerator," SLAC Report No. 14, Stanford Linear Accelerator Center, Stanford University, Stanford, California (1963).

7. R.H. Helm, "Misalignment and Quadrupole Error Problems Affecting the Choice of Multiplet Type for Sector Focusing of the Two-Mile Accelerator," SLAC Report No. 15, Stanford Linear Accelerator Center, Stanford University, Stanford, California (1963).

8. R.H. Helm and W.K.H. Panofsky, "Beam Dynamics of the Project M Accelerator," M Report No. 201, Stanford Linear Accelerator Center, Stanford University, Stanford, California (1960).

9. "Proposal for a Two-Mile Linear Electron Accelerator," Stanford University, Stanford, Calif.(1957).

10. W.B. Herrmannsfeldt, "Magnetic Shielding System for the Stanford Two-Mile Accelerator," Paper II-22 of IEEE Particle Accelerator Conference, Washington, D.C., March 10-12, 1965.

11. R.H. Helm, "Effects of Stray Magnetic Fields and RF Coupler Asymmetry in the Two-Mile Accelerator with Sector Focusing," SLAC Report No. 20, Stanford Linear Accelerator Center, Stanford University, Stanford, California (1963).

12. W.B. Herrmannsfeldt, "Linac Alignment Techniques," Paper A-2 of IEEE Particle Accelerator Conference, Washington, D.C., March 10-12, 1965.

13. See for example P.B. Wilson, "A Study of Beam Blow-up in Electron Linacs," HEPL Report No. 297, Hansen Laboratories of Physics, Stanford University, Stanford, California (June 1963).

14. R.H. Kingsland, Hughes Aircraft Co., Fullerton, California (private communication).

15. Daryl Reagan, Stanford Linear Accelerator Center (private communication).

16. O.H. Altenmueller, R.R. Larsen and G.A. Loew, "Investigations of Traveling-Wave Separators for the Stanford Two-Mile Linear Accelerator," SLAC Report No. 17, Stanford Linear Accelerator Center, Stanford University, Stanford, California (1963).

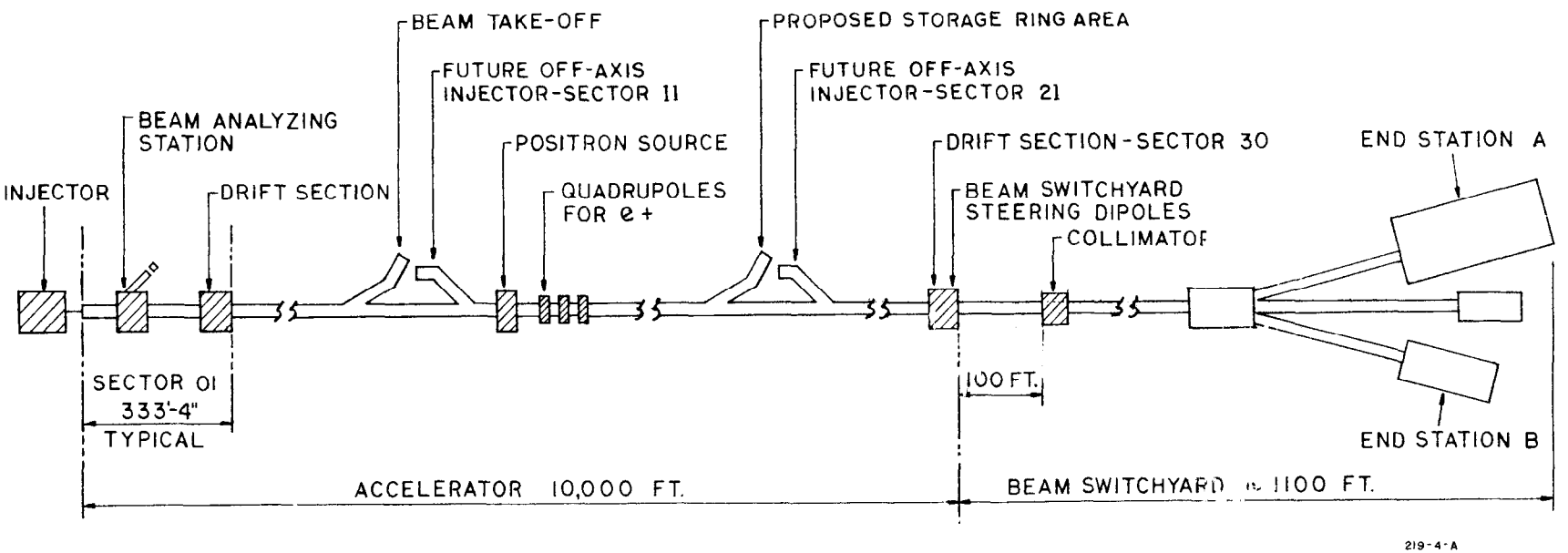


FIG. 1 - OVERALL LAYOUT OF THE TWO-MILE ACCELERATOR

$\theta$ = PHASE ANGLE OF CENTRAL ELECTRON WITH RESPECT TO WAVECREST.

$\alpha$ = ANGULAR PHASE SPREAD OF BUNCH.

a) EFFECT OF FINITE BUNCH SIZE.

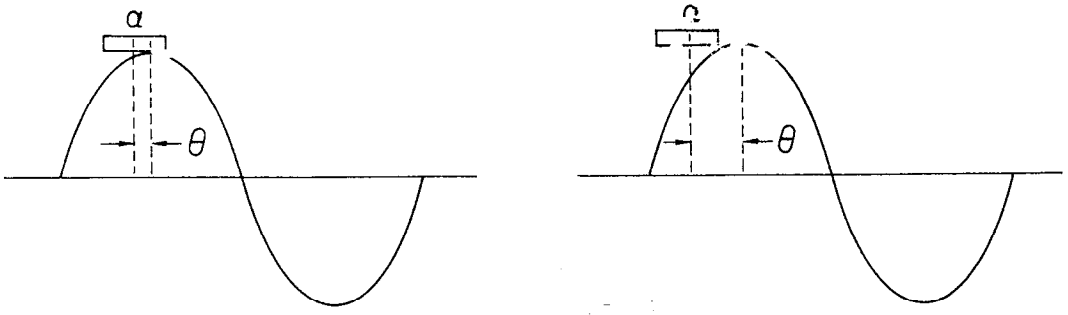


$|\theta| \leq \alpha/2 << 1$

$\frac{\Delta V}{V} \approx \frac{1}{2}\left(\frac{\alpha}{2} + |\theta|\right)^2$

$= \frac{\alpha^2}{8}$ FOR $\theta = 0$

$1 >> |\theta| \geq \alpha/2$

$\frac{\Delta V}{V} \approx |\theta|\alpha$

b) IMPERFECT PHASING WITHOUT PHASE CLOSURE

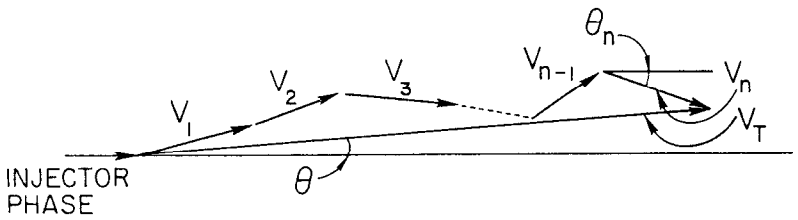


c) IMPERFECT PHASING WITH PHASE CLOSURE

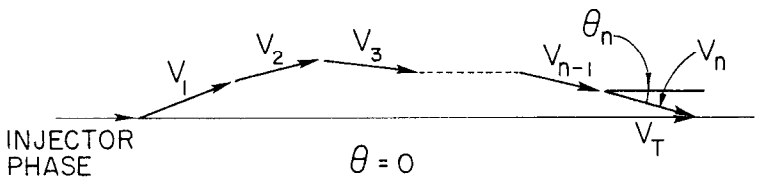


219-8-A

FIG. 2 - THE EFFECT OF FINITE BUNCH SIZE ON ENERGY SPECTRUM

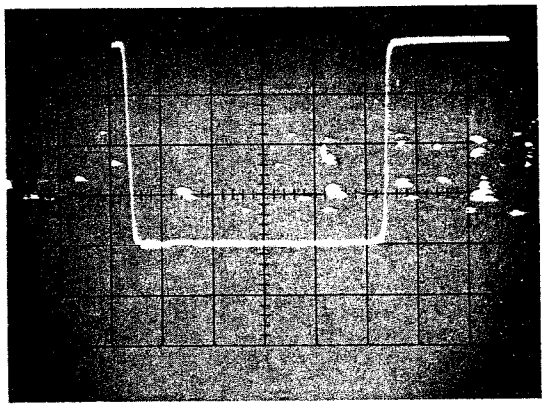

( a )

Input amplitude pulse

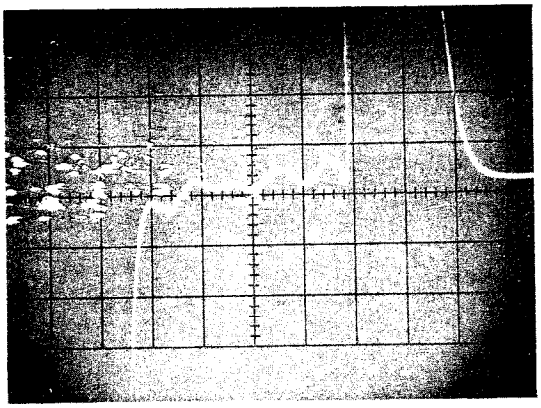

( b )

Input phase
(1 cm = 2.5 electrical degrees)

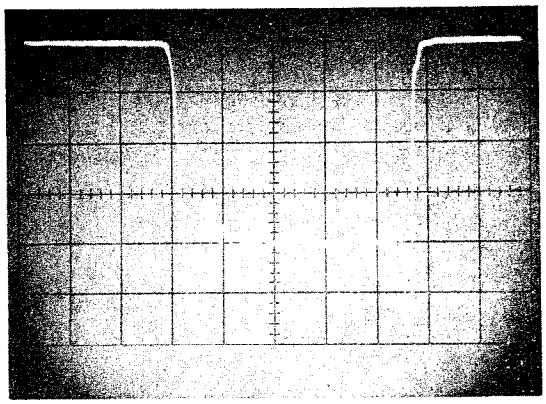

( c )

Output amplitude pulse

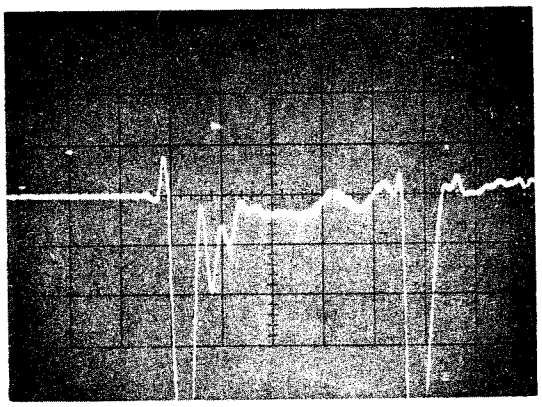

( d )

Output phase
(1 cm = 2.5 electrical degrees)

219-10-8

FIG. 3--Experimental measurements of amplitude and phase modulation at the input and output of an accelerator section (60 pps).

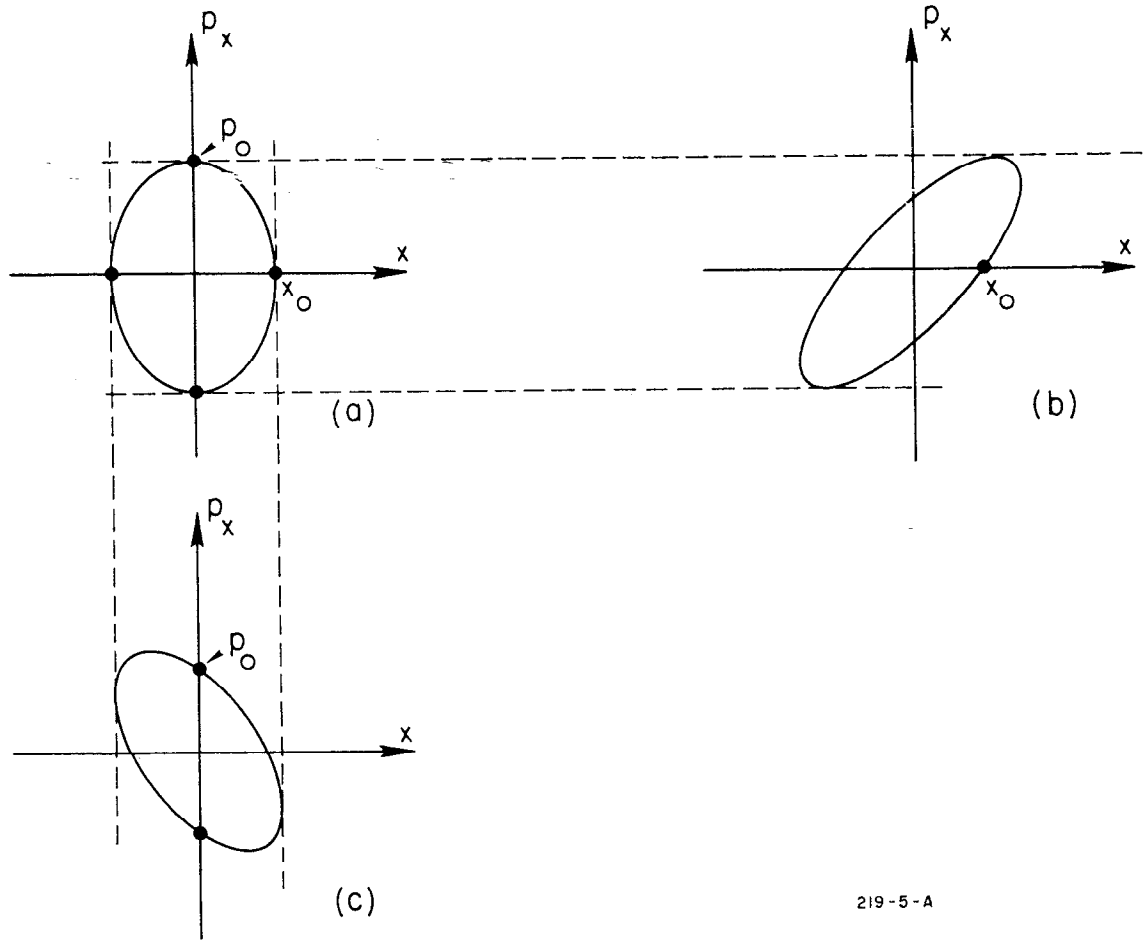


FIG. 4 - TYPICAL PHASE SPACE DIAGRAMS USED IN DISCUSSIONS OF BEAM TRANSPORT.

(a) EQUIVALENT ERECT ELLIPSE

(b) TRANSFORMED BY A DRIFT LENGTH.

(c) TRANSFORMED BY A THIN CONVERGING LENS.

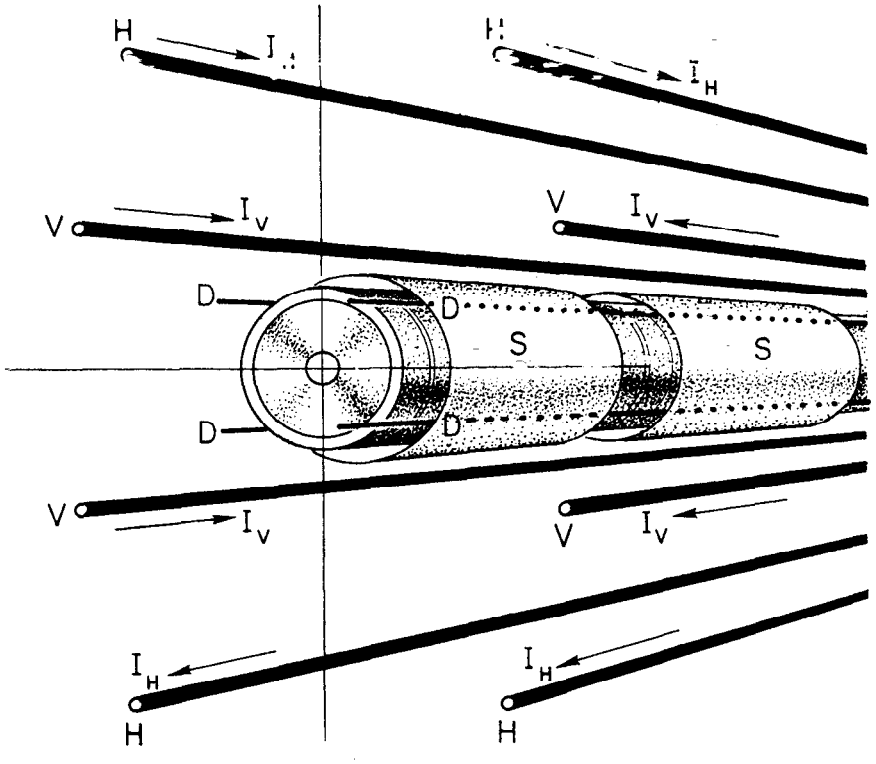


V = VERTICAL FIELD DEGAUSSING WIRES
H = HORIZONTAL FIELD DEGAUSSING WIRES
S = SHIELDING
D = DEMAGNETIZING WIRES

224-1-A

FIG. 5 - CROSS-SECTION OF DEGAUSSING AND MAGNETIC SHIELDING SYSTEM

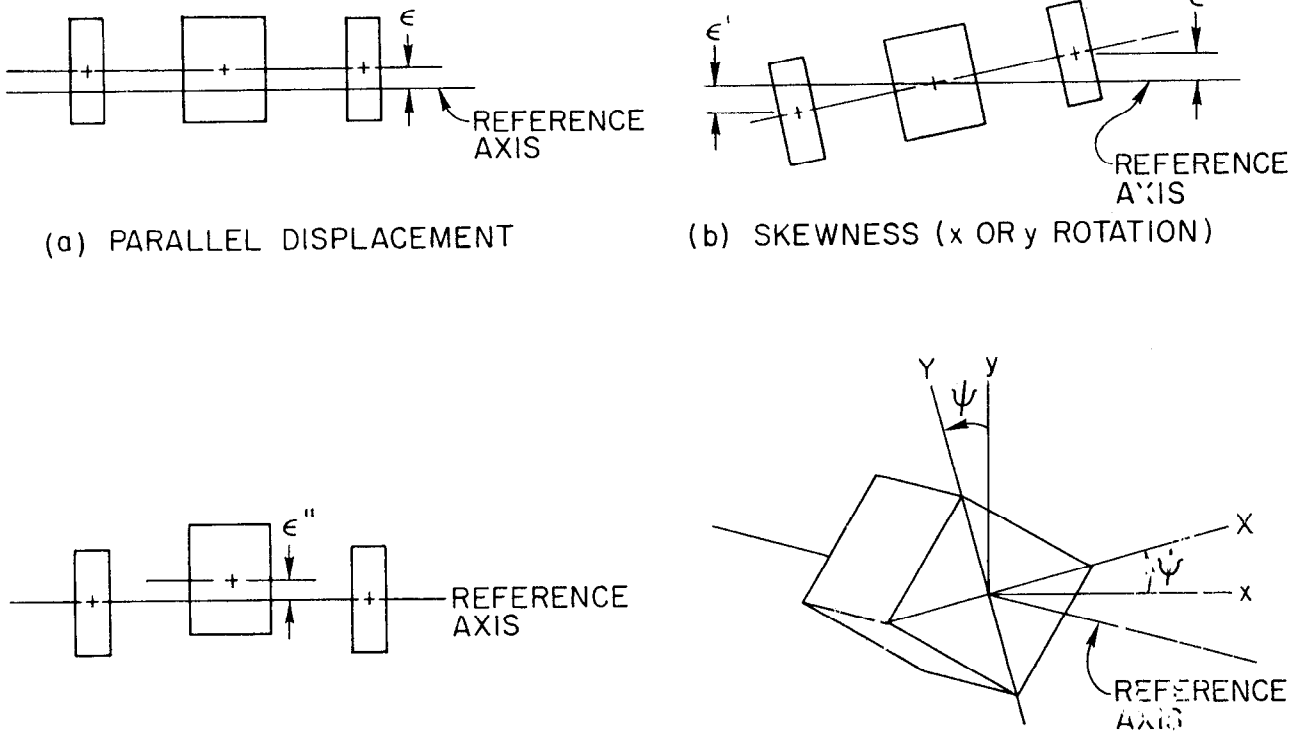


FIG. 6 - ILLUSTRATION OF TRIPLET MISALIGNMENT COMPONENTS.

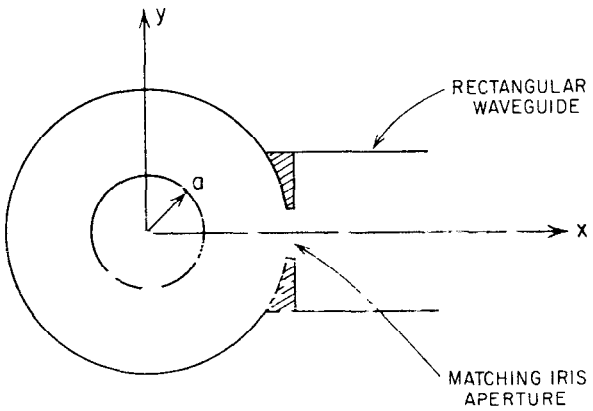


a.) CROSS-SECTION OF COUPLER CAVITY

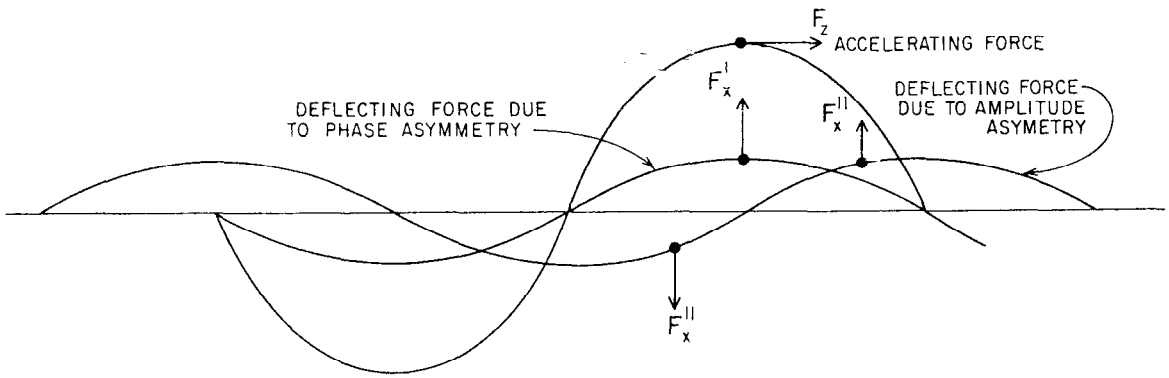


b.) FORCE COMPONENTS DUE TO AMPLITUDE AND PHASE ASSYMMETRY IN THE COUPLER CAVITIES

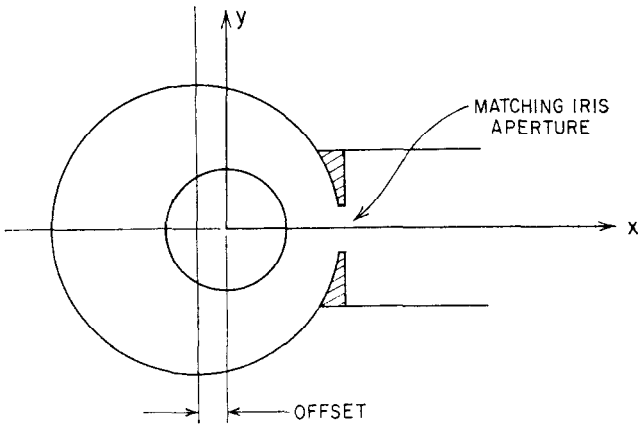


c.) COUPLER OFFSET TO CORRECT AMPLITUDE ASYMMETRY

185-1-A

FIG. 7 -THE COUPLER ASYMMETRY PROBLEM

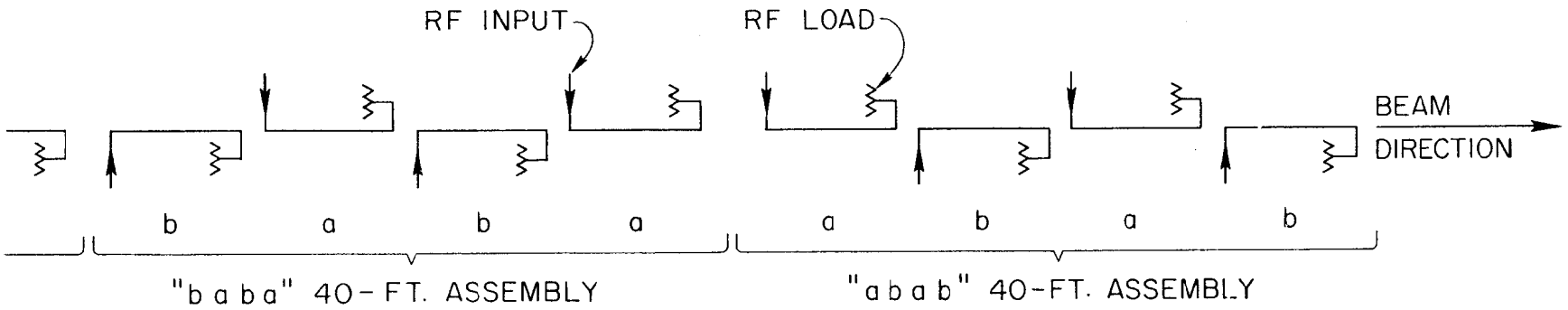


a. SCHEMATIC OF "b a b a - a b a b" WAVEGUIDE CONFIGURATION. EACH 40-FT. ASSEMBLY IS POWERED BY A SINGLE KLYSTRON.

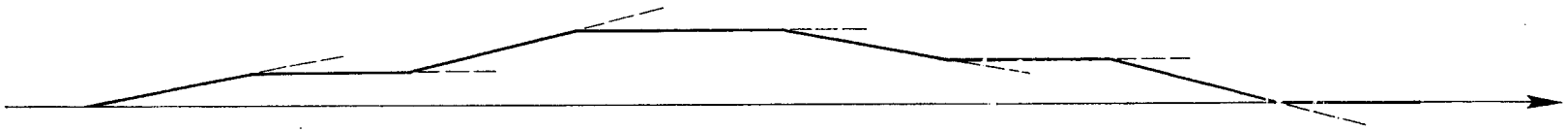

b. SCHEMATIC OF BEAM TRAJECTORY WITH "b a b a - a b a b" CONFIGURATION, SHOWING CANCELLATION OF DEFLECTION AT 80-FT. INTERVALS.

219-2-A

FIG. 8 - THE "b a b a - a b a b" WAVEGUIDE FEED CONFIGURATION AND RESULTING BEAM DISPLACEMENT.

a)

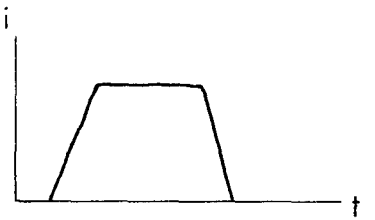


GUN CURRENT PULSE

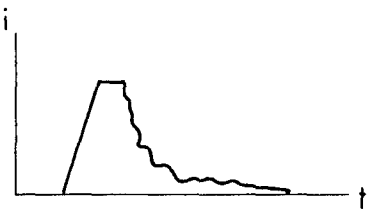


BROKEN-UP ACCELERATOR CURRENT PULSE

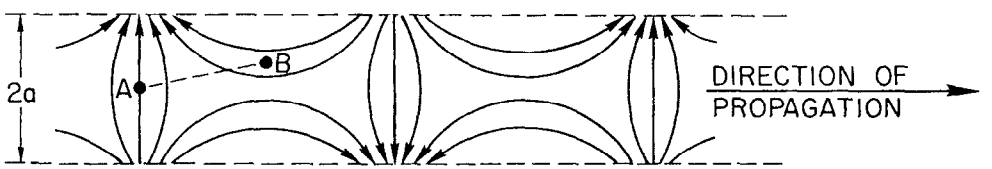


b) SNAPSHOT OF THE LORENTZ FORCE FIELD ($E+\beta \times B$) OF THE DEFLECTING ($TM_{11}$-LIKE) FUNDAMENTAL MODE.

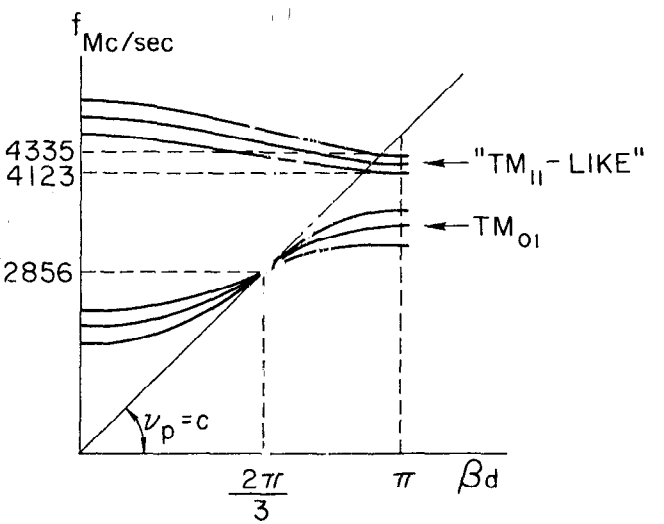


c) $TM_{01}$ AND $TM_{11}$-LIKE MODES FOR THE SLAC CONSTANT-GRADIENT STRUCTURE.

FIG. 9 - BEAM BREAK-UP PHENOMENOM

219-7-A

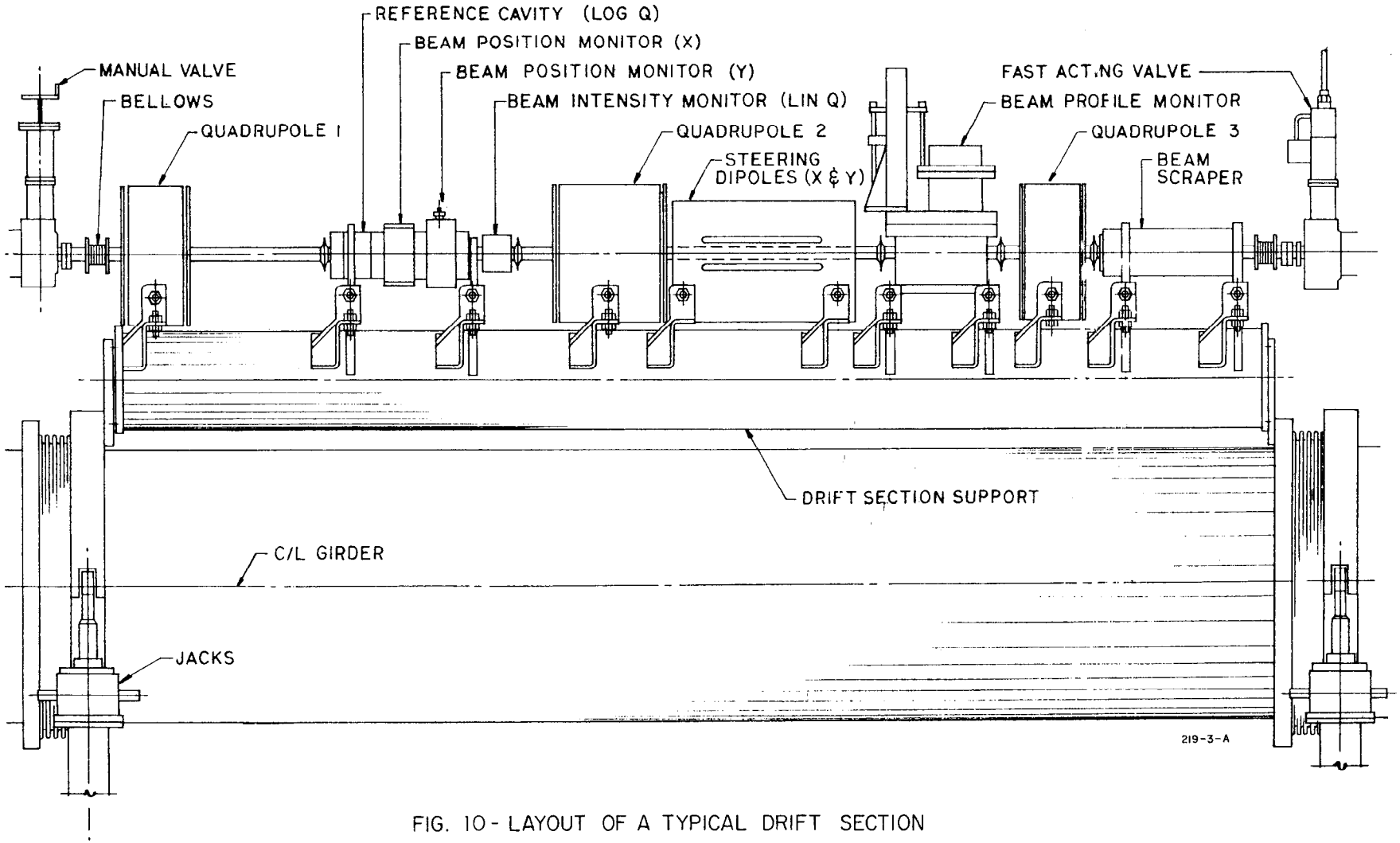


FIG. 10 - LAYOUT OF A TYPICAL DRIFT SECTION

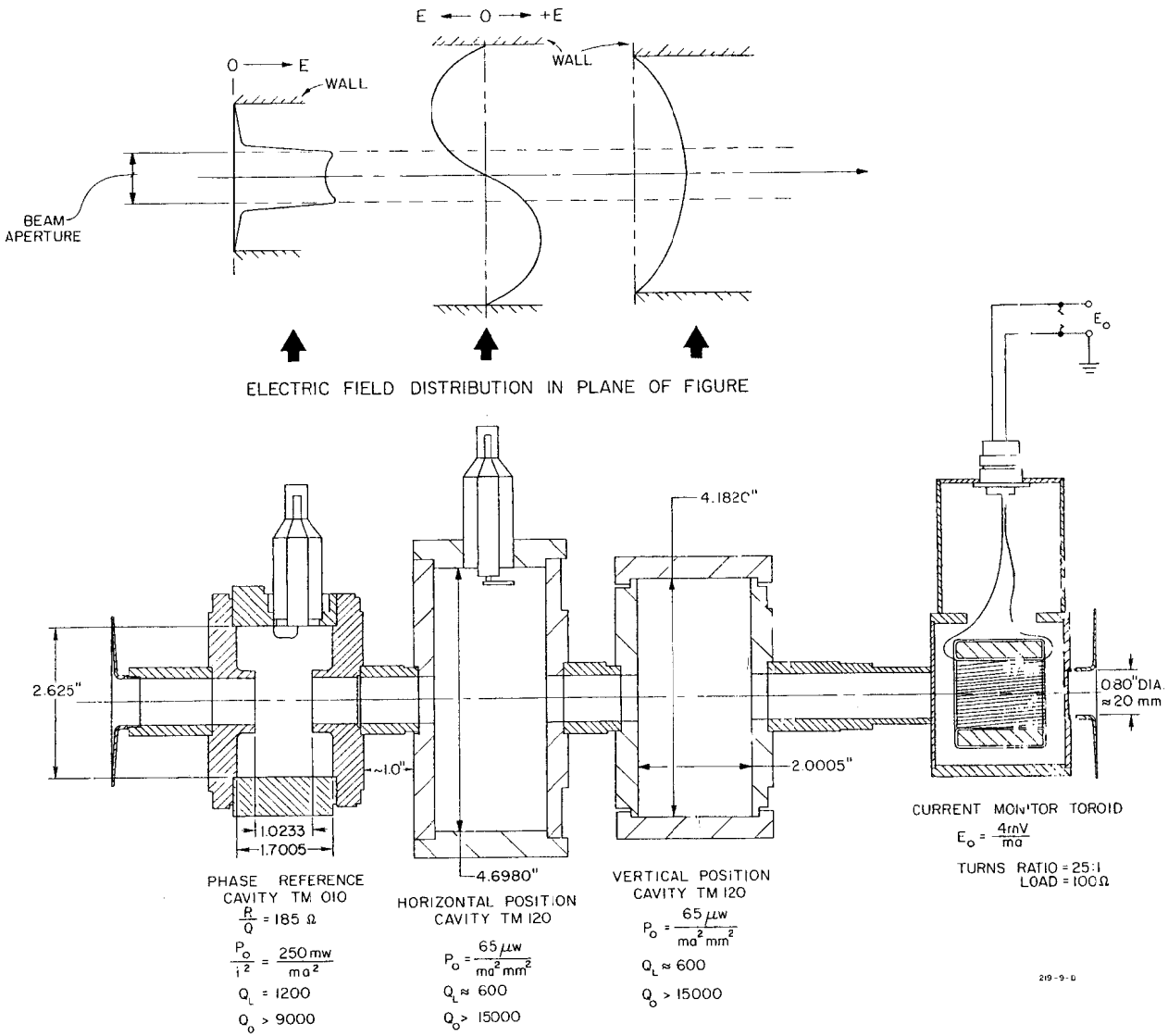


FIG. 11 - BEAM INTENSITY AND POSITION MONITORS (TOP VIEW)

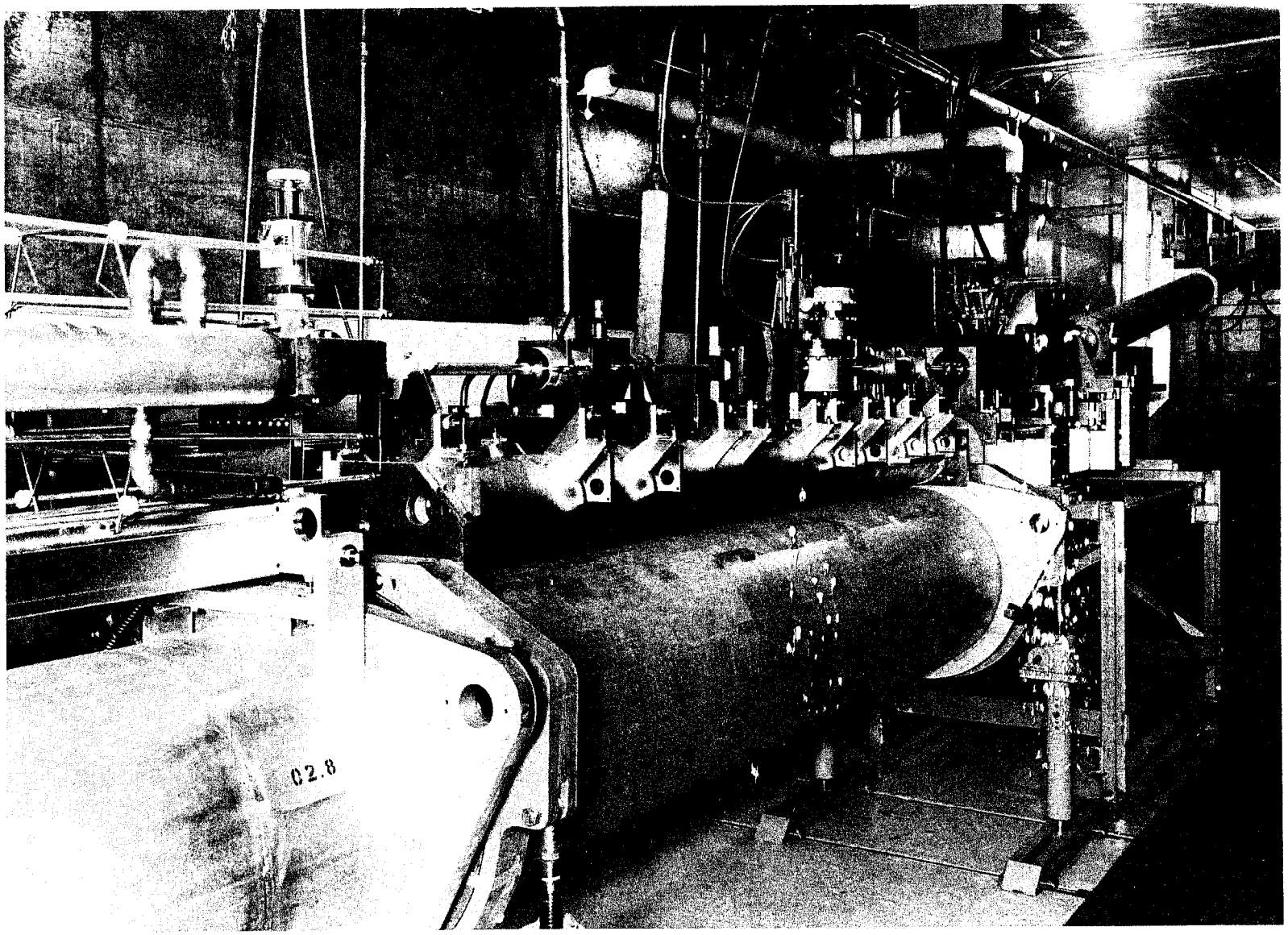


FIG. 12--Temporary beam analyzing station at the end of Sector 2.